Available online at www.sciencedirect.com

ScienceDirect

Procedia CIRP 31 (2015) 58 – 63

www.elsevier.com/locate/procedia

15th CIRP Conference on Modelling of Machining Operations

Variable compliance-related aspects of chatter in turning thin-walled tubular parts

Artem Gerasimenko[a,b], Mikhail Guskov[a], Jérôme Duchemin[a], Philippe Lorong[a,*], Alexander Gouskov[b]

[a] *PIMM Laboratory, Arts et Metiers ParisTech, 151 bd de l'Hopital, Paris 75013, France*
[b] *Bauman Moscow State Technical University, 2-eme Baumanskaya, 5, Moscow 105005, Russia*

* Corresponding author. Tel.: 33-1-44246285. *E-mail address:* philippe.lorong@ensam.eu

Abstract

Thin tubular parts are often subject to turning process during manufacturing. The increasing compliance of the workpiece, which is associated to tool displacement and to matter removal, can give rise to chatter, leading to poor surface quality or premature machine/tool damage. The present work addresses an experimental case of turning a steel thin-walled tube featuring intense vibrations with variable parameters. Observations of transient records during the pass suggest a strong influence of the matter removal on the eigenfrequencies of the system, while the tool's motion implies strong variation of the modal projection of the cutting force. Another characteristic phenomenon is the intermittency of the vibrations and discontinuous chatter frequency evolution. These phenomena are reproduced and analyzed numerically. By means of a finite element modeling, the part's geometry variation during the pass is taken into account. Finally, a stability analysis is carried out for several states of this evolutive system in order to gather insight into the steady cutting conditions.

Peer-review under responsibility of the International Scientific Committee of the "15th Conference on Modelling of Machining Operations

Keywords: Turning; Chatter ; Predictive Model.

1. Introduction

Stability of quasi-stationary cutting, such as turning or drilling, is a subject studied since a long time. In 1958, Tobias [1] has proposed a delay-based description of regenerative chatter mechanism which has since been widely used, especially in the framework of so-called stability lobes diagrams based on Laplace domain analysis. Recent versions of SDOF and MDOF protocols for stability lobes construction can be found in textbooks by Altintas [6] or Cheng [7].

In practice, most turning stability studies concern cases of massive parts, representable by rigid solid or rod models. A recent review of these methods is provided by Siddhpura and Paurobally [8]. Nevertheless, thin-walled parts constitute a particular subject that is also addressed in literature, although scarcely. In a work of Arnold, 1961 [9] an experimental study of steel tubular parts (gun cradles) reveals multiple zones subject to vibrations during turning. In 2002, Mehdi et al. [10, 11] have investigated aluminum tubular parts turning via numerical or analytical part modeling and experimental tests for various cutting conditions. In 2011, Lorong et al. [12] have presented an experiment accompanied with full time domain simulations featuring strong chatter and bringing forward the impact of the damping on the instability onset. All of these works highlight the importance of the damping on the onset of instability. Another important aspect for thin-walled structures is the frequent occurrence of strong changes in the workpiece dynamical stiffness and eigenfrequencies during one pass.

In this paper we focus on the straight turning of a thin tubular part. As it is often the case of thin-walled workpieces, the matter removal leads to a significant variation of stiffness and eigenfrequencies of the part and plays a major role in the observed phenomena. The investigation concerns a pass featuring multiple regenerative chatter instabilities. We propose to use a stability approach to figure out different aspects of the experimental observations on the machined surface and measured vibrations.

In section 2 we present the design of the experiment, chosen in order to have an increase in compliance of workpiece while the tool progresses. After this description of the experimental setup, the section 3 presents the numerical modeling approach, based on evolutive FE models. In section 4, the stability analysis methodology including modal decomposition is explained. Finally, the application to the present case is depicted in section

Peer-review under responsibility of the International Scientific Committee of the "15th Conference on Modelling of Machining Operations
doi:10.1016/j.procir.2015.03.088

5 and the results are presented and discussed in the section 6.

2. Experimental setup and measurements

On the cross-section given on Figure 1 one can see the shape of the machined tube. The horizontal axis is the revolution axis of the workpiece. On this figure one can also see the contact point $P(t)$ between the tool and the workpiece, where t stands for the time, evolving from the left to right at a constant speed, feed per revolution f and rotational speed Ω of the workpiece being constant. The more the tool goes to the right the more the workpiece is flexible. On Figure 1 is also represented the cut section whose area is equal to $a_p\, f = b\, h$, where a_p is the depth of cut, h is the cut thickness and b the width of cut. Those last quantities are linked with the cutting edge angle κ_r: $b \sin\kappa_r = a_p$ and $f \sin\kappa_r = h$. This operation was carried out with a square insert (Sandvik SCMT 432-PR). Lastly two direct orthonormal bases are defined on Figure 1: $(\mathbf{n}, \mathbf{a}, \mathbf{g})$ linked to the rake face and cutting edge of the tool (defined and used in section 3.2) and $(\mathbf{x}, \mathbf{y}, \mathbf{z})$ linked to the tool, $\mathbf{x}$ being the revolution axis of the workpiece and the feed direction, $\mathbf{y}$ being in the radial direction and $\mathbf{z}$ being tangent to the tube circumference. In the studied case, $\mathbf{n}$ and $\mathbf{z}$ are identical.

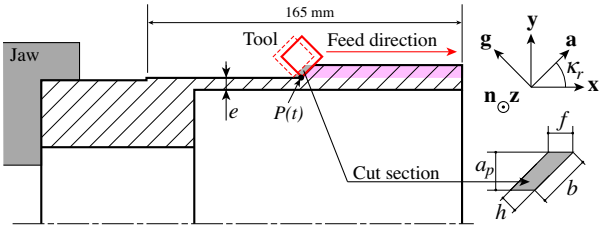

Fig. 1. Geometry of the machined tube – Cut section and associated bases

Figure 2 shows the machined surface with chatter marks, resulting from the experiment under consideration. Several stripe-shaped zones of chatter defects are distinguishable. These zones can be clearly associated to recorded vibration bursts presented below (Figure 8). The radial depth of the defects is amounts to 0.2 mm at maximum (free end of the shell).

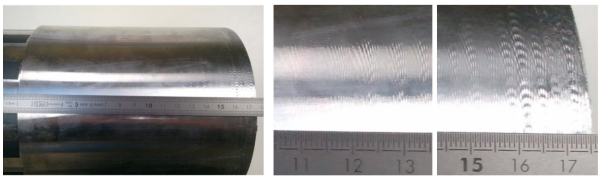

Fig. 2. Surface of the tube after the last tool path

The experimental set up is shown in Figure 3. Some of the measurements made during the experiment were done to verify that the workpiece is the weak part of the system. That is the case, for example, with accelerometer 'a1' on spindle support and with the two accelerometers 'a2' and 'a3' on the tool (Figure 3). The optic sensor 'o1' (Figure 3) was used to obtain an accurate value of the rotational rate of the spindle. This value is $\Omega = 79.39 \pm 0.02$ rad/s (758.15 ± 0.2 rev/min) which correspond to a period $T = 79.14 \pm 0.02$ ms. It also helped to verify that we have no significant variation of Ω during the machining.

During the test we have made several tool paths until vibrations were observed during machining. It is this last path that is concerned by our investigation. These vibrations generated defects on the machined surface as it is visible on Figure 2. This occurred for a thickness e of the tube going from 5.4 mm to 4.4 mm. Before and after this last path a hammer test gave us the 2 transfer functions (the impacts were applied near accelerometer 'a5' while the latter gave the response, Figure 3) given Figure 4. The experimental data given in table 2 and table 3 are coming from these transfer functions.

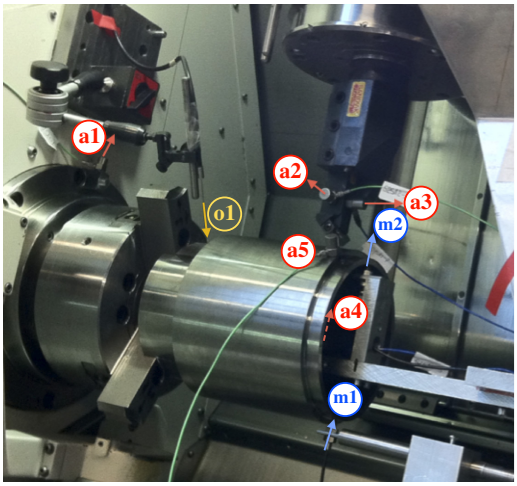

Fig. 3. Experimental setup

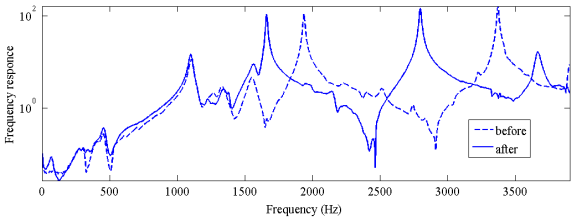

Fig. 4. Transfer function before and after the last tool path

For the measurement of the workpiece vibration *during machining* we used the eddy current sensor 'm1' fixed on the machine frame. This sensor is placed in front of the right extremity of the workpiece where the largest displacements are present. The evolution of the workpiece surface displacement measured at this point is given at the bottom of Figure 8. On the right side of this graphic the observed oscillations correspond to those visible on the workpiece surface on Figure 2. On the spectrogram computed from this displacement curve from the 'm1' sensor (Figure 5) one can see the evolution of the resonance of the tube close to the evolution of its eigenfrequencies.

On Figure 3 one can also see the eddy current sensor 'm2' but due to presence of chips inside the tube the data this sensor

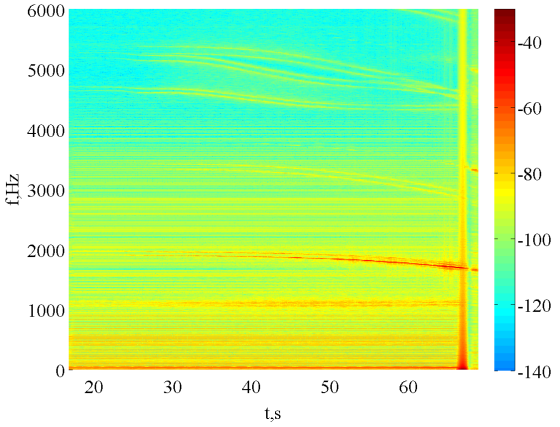

Fig. 5. Spectrogram issued from the measurement of the eddy current sensor 'm1', dB

accumulated was not exploitable. Accelerometer 'a4' was positioned on 'm2' sensor support to measure the vibrations of this support.

3. Numerical models

3.1. Dynamic model of the workpiece

The dynamic behavior of the workpiece is based on a 3D finite element model using 10 nodes parabolic tetrahedrons (Figure 6). The material data (C38 steel) are: Young modulus $E = 2.1\text{e}11\,\text{Pa}$, density $\rho = 7\,800\,\text{kg/m}^3$, poisson coefficient $\nu = 0.3$. This model allows to take into account the effect of the

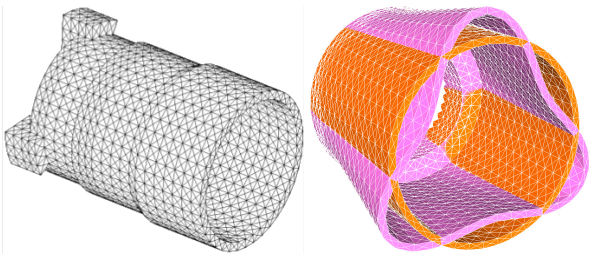

Fig. 6. Finite element model. Left: workpiece mesh for a machining evolution at the middle of workpiece. Right: eigenmode of interest

tool progression as matter removal modifies the thickness of the workpiece, an thus its mass and stiffness. On Figure 6 (left) one can see the thickness variation (with noticeable exaggeration on this figure in order to render it clearly visible).

During the progression of the tool the eigenfrequencies of the system are changing. In table 2 the five first eigenfrequencies are given for different steps of the tool progression going from the beginning of the machining, 0 mm, to its end, 165 mm. Due to the cyclic symmetry of the system (tube and clamping) non axial or torsional modes are twin modes.

Table 2 and table 3 list the values of the eigenfrequencies, as well as modal damping factors, issued from the experiment (curves on Figure 4), before and after the last path of the tool.

Table 1. Eigenfrequency evolution (Hz) during tool progression

Modal form					Order
2 lobes	1102	1084	1089	1108	1&2
1 flexion	1567	1552	1579	1658	3&4
3 lobes	1943	1914	1849	1672	5&6
4 lobes	3386	3365	3208	2827	7&8
torsion	2909	2923	2980	3070	9
Progress (mm) :	0	55	115	165	

Table 2. Experimental and numerical eigenfrequencies before tool passage

Frequency Exp. (Hz)	1108.4	1937.2	3384.5
Frequency FE (Hz)	1102	1943	3386
Error (%)	-0.58	0.30	0.04
Modal damping	0.0105	0.00076	0.00051
Modal form	2 lobes	3 lobes	flexion 2

The comparison with numerical values are also given showing that numerical and experimental eigenfrequencies are quite close.

Table 3. Experimental and numerical eigenfrequencies after tool passage

Frequency Exp. (Hz)	1100.2	1661.1	2798
Frequency FE (Hz)	1108	1672	2827
Error (%)	0.7	0.66	1.04
Modal damping	0.0077	0.00070	0.00078
Modal form	2 lobes	3 lobes	4 lobes

3.2. Cutting law

We choose to utilize a Kienzle cutting law [5][4] in order to determine the cutting forces applied on the workpiece with respect to the depth of cut h and the width of cut b (Fig. 1). For each component of the cutting force, this kind of cutting law uses 2 parameters:

$$F_j = K_j\,\tilde{b}\,\tilde{h}^{n_j} \quad \text{with} \quad \tilde{b} = \frac{b}{h_0},\ \tilde{h} = \frac{h}{h_0},\quad j \in \{n, a, g\} \tag{1}$$

The reference length $h_0 = 1\,mm$ is used to achieve a dimensionless form for the the cutting law. Specific cutting pressures K_j are in Newton. The three components F_j are defined in the basis $(\mathbf{n}, \mathbf{a}, \mathbf{g})$ (Fig. 1) associated to the rake face of the tool:

- $\mathbf{n}$: unit outward normal to the rake face (here supposed to be flat),
- $\mathbf{a}$: unit vector parallel to the cutting edge,
- $\mathbf{g}$: unit vector parallel to the rake face and perpendicular to $\mathbf{n}$ and $\mathbf{a}$ and directed towards the tool.

The basis $(\mathbf{n}, \mathbf{a}, \mathbf{g})$ is direct.

$$\mathbf{F} = F_n\,\mathbf{n} + F_a\,\mathbf{a} + F_g\,\mathbf{g} \tag{2}$$

The used coefficients of the cutting law are given in the table 4.

Table 4. Kienzle cutting law coefficients

Component	$K_j(N)$	n_j
F_n	1278.	0.5843
F_a	0.0	0.0
F_g	402.8	0.3405

4. Stability analysis

4.1. Equation of perturbed motion

In the studied example, the system is very close to an axisymmetric problem. In this context, as it is often the case in turning, the analysis can be carried out in the fixed [global inertial] frame $\mathcal{R}_o$, with respect to which the cutting process is driven by a frequency Ω (workpiece rotation rate).

In this frame the FE model conducts to the classical matrix equation of motion :

$$\mathbf{M}\ddot{\mathbf{q}}(t) + \mathbf{D}\dot{\mathbf{q}}(t) + \mathbf{K}\mathbf{q}(t) = \mathbf{f}_c(t, \mathbf{q}(t) - \mathbf{q}_T(t), \dot{\mathbf{q}}(t)). \tag{3}$$

where $\mathbf{M}$, $\mathbf{D}$, and $\mathbf{K}$ stand for mass, generalized damping and stiffness matrices of the unloaded system respectively, t time variable, $\mathbf{q}$, $\mathbf{f}_c$, mean generalized displacements and load forces vectors respectively, $T = \dfrac{2\pi}{\Omega}$ delay due to the cutting interaction history and $\mathbf{q}_T(t) = \mathbf{q}(t - T)$. The loads $\mathbf{f}_c$ are induced by the tool-workpiece interaction. Let n be the size of this system, n is the number of degrees of freedom of the FE model. The matrices $\mathbf{D}$ and $\mathbf{K}$ may contain non galilean effects such as Coriolis effect due to workpiece rotation [2].

To analyze the stability of a given reference solution

$$\mathbf{q} = \mathbf{q}_0 \tag{4}$$

satisfying the equation (3), the perturbed motion $\mathbf{q}$ is studied:

$$\mathbf{q} = \mathbf{q}_0 + \mathbf{p}; \quad \dot{\mathbf{q}} = \dot{\mathbf{q}}_0 + \dot{\mathbf{p}}; \quad \ddot{\mathbf{q}} = \ddot{\mathbf{q}}_0 + \ddot{\mathbf{p}} \tag{5}$$

with $\mathbf{p}$ standing for the perturbation.

In case of turning, $\mathbf{q}_0$ is a constant resulting from steady-state deflection under nominal tool-workpiece interaction. For small $\mathbf{p}$, a linearized problem can be derived from (3), by subtracting the reference ($\mathbf{q}_0$-related) part due to (4):

$$\mathbf{M}\ddot{\mathbf{p}} + \mathbf{D}\dot{\mathbf{p}} + \mathbf{K}\mathbf{p} = \frac{\partial \mathbf{f}_c}{\partial \mathbf{q}}\mathbf{p} + \frac{\partial \mathbf{f}_c}{\partial \dot{\mathbf{q}}}\dot{\mathbf{p}} + \frac{\partial \mathbf{f}_c}{\partial \mathbf{q}_T}\mathbf{p}_T. \tag{6}$$

As $\dfrac{\partial \mathbf{f}_c}{\partial \mathbf{q}_T} = -\dfrac{\partial \mathbf{f}_c}{\partial \mathbf{q}}$ and with $\mathbf{K}_c = -\dfrac{\partial \mathbf{f}_c}{\partial \mathbf{q}}$ and $\mathbf{D}' = \mathbf{D} - \dfrac{\partial \mathbf{f}_c}{\partial \dot{\mathbf{q}}}$ we finally have:

$$\mathbf{M}\ddot{\mathbf{p}}(t) + \mathbf{D}'\dot{\mathbf{p}}(t) + \mathbf{K}\mathbf{p}(t) = -\mathbf{K}_c\left(\mathbf{p}(t) - \mathbf{p}(t - T)\right). \tag{7}$$

The Laplace transform of (7) would yield:

$$\left[s^2\,\mathbf{M} + s\mathbf{D}' + \mathbf{K} + \mathbf{K}_c\left(1 - e^{-sT}\right)\right]\mathbf{P} = 0. \tag{8}$$

4.2. Stability threshold

The cutting operation under consideration is defined by the workpiece rotation velocity Ω and by a cut depth-related parameter that we will note p and it is on the plane Ω—p that the stable zones are sought. The parameter p is classically [3] related to the chip width b (Fig. 1) and we have then $\mathbf{K}_c = p\mathbf{K}_{c0}$.

Then, by introducing the dynamic stiffness matrix function $\mathbf{Q}(s)$ of the unloaded system

$$\mathbf{Q}(s) = (s^2\mathbf{M} + s\mathbf{D}' + \mathbf{K}) \tag{9}$$

and by enforcing the stability threshold condition (zero-real part of s) $s = \mathbf{i}\omega$, the equation of perturbation in the Laplace domain (8) can be rewritten as follows:

$$(\mathbf{Q}(\mathbf{i}\omega) - p(1 - e^{-\mathbf{i}\omega T})\mathbf{K}_{c0})\mathbf{P} = 0 \tag{10}$$

or in a more compact way:

$$(\mathbf{Q}(\mathbf{i}\omega) - \lambda\mathbf{K}'_{c0})\mathbf{P} = 0; \tag{11}$$

with

$$\lambda = p(1 - e^{-\mathbf{i}\omega T}) \tag{12}$$

Thus, for given ω, one can compute λ from the eigenproblem (11). As p is a positive real, after representing λ in exponential form:

$$\lambda = \lambda_0 e^{\mathbf{i}\psi}, \tag{13}$$

one can state the following condition:

$$\mathrm{Im}\left((1 - e^{-\mathbf{i}\omega T})e^{-\mathbf{i}\psi}\right) = 0 \tag{14}$$

which would yield $\sin(\omega T + \psi) - \sin\psi = 0$ giving place to two possibilities:

$$\begin{array}{lrcl} 1. & \omega T & = & 2\pi k \\ 2. & \omega T + \psi & = & \pi - \psi + 2\pi k \end{array} \tag{15}$$

with $k \in \mathbb{Z}$. The first option in (15), corresponding to $\lambda = 0$, is of no practical interest. The second case in (15) gives the following relationship between ω and T:

$$\omega T = -2\psi + (2k + 1)\pi, \quad k \in \mathbb{Z} \tag{16}$$

Here the index k defines the instability harmonic number. Finally, a value of p can be found from (12) and (16).

4.3. Working in a modal basis

In order to reduce the size of the dynamical problem it is very interesting, and classical, to use a truncated modal basis $\mathbf{\Phi} = [\phi_1, \phi_2, \ldots, \phi_N]$ composed of N eigenmodes ϕ_i coming from the homogeneous conservative system $\mathbf{M}\ddot{\mathbf{q}} + \mathbf{K}\mathbf{q} = \mathbf{0}$ so as to approximate $\mathbf{q}$ and
vp:

$$\mathbf{q} \approx \mathbf{\Phi}\,\overline{\mathbf{q}} \quad \text{and} \quad \mathbf{p} \approx \mathbf{\Phi}\,\overline{\mathbf{p}} \tag{17}$$

with

$$\overline{\mathbf{q}}^T = \langle \overline{q}_0, \overline{q}_1, \ldots \overline{q}_N \rangle \quad \text{and} \quad \overline{\mathbf{p}}^T = \langle \overline{p}_0, \overline{p}_1, \ldots \overline{p}_N \rangle. \tag{18}$$

In this modal basis the stability eigenproblem (11)can be rewritten as:

$$\left(\overline{\mathbf{Q}}(\mathbf{i}\omega) + \lambda\overline{\mathbf{K}}_{c0}\right)\overline{\mathbf{P}} = \mathbf{0} \tag{19}$$

with

$$\overline{\mathbf{Q}}(\mathbf{i}\omega) = \mathbf{\Phi}^T(-\omega^2\,\mathbf{M} + \mathbf{i}\omega\mathbf{D}' + \mathbf{K})\mathbf{\Phi} \quad \text{and} \quad \overline{\mathbf{K}}_{c0} = \mathbf{\Phi}^T\mathbf{K}_{c0}\mathbf{\Phi}. \tag{20}$$

4.4. Computation of $\overline{\mathbf{K}}_{c0}$

In the FE framework the displacement interpolation, at any point M of the structure, can be written in the following form :

$$\mathbf{u}(M,t) = \mathbf{N}(M)\mathbf{q}(t) \tag{21}$$

where $\mathbf{u}(M,t)$ is the column containing the 3 components of the displacement vector at M and t, $\mathbf{N}(M)$ is the rectangular $[3 \times n]$ matrix of the FE shape function at M.

In turning the action of the tool on the workpiece can be modeled by a unique cutting force vector $\vec{F}_c$ applied on the contact point P between the tool and the workpiece. This cutting force vector conducts, in the FE approach, to the generalized cutting force column $\mathbf{f}_c$ defined by :

$$\mathbf{f}_c(t) = \mathbf{N}^T(P)\,\mathbf{F}_c(t) \tag{22}$$

present in eq. (3) and where $\mathbf{F}_c$ is the column containing the 3 components of $\vec{F}_c$. The cutting stiffness matrix $\mathbf{K}_c$ can then be compute in the following way

$$-\mathbf{K}_c = \frac{\partial \mathbf{f}_c}{\partial \mathbf{q}} = \frac{\partial \mathbf{f}_c}{\partial \mathbf{u}(P)}\frac{\partial \mathbf{u}(P)}{\partial \mathbf{q}} = \mathbf{N}^T(P)\frac{\partial \mathbf{F}_c}{\partial \mathbf{u}(P)}\mathbf{N}(P) \tag{23}$$

and thus finally

$$-\mathbf{K}_c = \frac{\partial \mathbf{f}_c}{\partial \mathbf{q}} = \frac{\partial \mathbf{f}_c}{\partial \mathbf{u}(P)}\frac{\partial \mathbf{u}(P)}{\partial \mathbf{q}} = \mathbf{N}^T(P)\frac{\partial \mathbf{F}_c}{\partial \mathbf{u}(P)}\mathbf{N}(P) \tag{24}$$

$$\overline{\mathbf{K}}_{c0}(P) = -\frac{1}{p}\mathbf{\Phi}^T\mathbf{N}^T(P)\frac{\partial \mathbf{F}_c}{\partial \mathbf{u}(P)}\mathbf{N}(P)\mathbf{\Phi}. \tag{25}$$

$\frac{\partial \mathbf{F}_c}{\partial \mathbf{u}(P)}$ is a $[3 \times 3]$ square matrix, and the rank of this matrix would define the rank of the modal matrix $\overline{\mathbf{K}}_{c0}$. Two properties of this matrix are of interest for our investigation:

- the local apparent cutting stiffness depends on the tool position (point P) and thus evolves during the machining of the tube,
- for a given ω, the number of eigenvalues in the eigenproblem (19) cannot be greater than 3.

5. Application to tube turning case

A preliminary analysis accounting for 10 first eigenmodes has shown that the mode corresponding to the observed chatter frequency systematically features the lowest stability threshold in terms of apparent cutting stiffness. Thus, for a detailed investigation, only that eigenmode has been retained.

This mode is the first 3 lobes eigenmode (Fig. 6, right).This eigenmode, and in fact all the eigenmodes having a low level damping (and corresponding with multi-lobes eigenmodes) exhibits the following properties :

- $u_x = \mathbf{u} \cdot \mathbf{x} \approx 0$
- $\frac{\partial \mathbf{F}_c}{\partial u_z} << \frac{\partial \mathbf{F}_c}{\partial u_x}$ and $\frac{\partial \mathbf{F}_c}{\partial u_z} << \frac{\partial \mathbf{F}_c}{\partial u_y}$

we have thus to compute only $k_0 = \frac{\partial \mathbf{F}_c}{\partial u_y}$ in the direction of radial displacement, i.e. radial stiffness. The orientation of the basis $(\mathbf{n}, \mathbf{a}, \mathbf{g})$ with respect to the basis $(\mathbf{x}, \mathbf{y}, \mathbf{z})$ is defined via κ_r (Figure 1).

The tool displacement (motion of point P) would induce not only a variation of the apparent modal cutting stiffness $\overline{\mathbf{K}}_{c0}(P)$ but also of the dynamic behavior of the workpiece. All matrices $\mathbf{M}$, $\mathbf{D}$, $\mathbf{K}$ evolve with the position of P. Indeed, the matter removal causes an evolution in eigenfrequencies and mode shapes. Thus for any position of P a particular stability lobes diagram has to be computed.

A cubic polynomial interpolation has been applied to the data from Table 1 in order to approximate the evolution of the eigenfrequency as well as of the radial component of the eigenmode under the tool during the pass, i.e. as a function of the tool position along the $\mathbf{x}$ axis. The resulting reduced system is described by a SDOF equation:

$$\ddot{\mathbf{p}} + 2\omega(x)\,\zeta\,\dot{\mathbf{p}} + \omega^2(x)\,\mathbf{p} = k_0\,\phi^2(x)\,(\mathbf{p}_T - \mathbf{p}), \tag{26}$$

here $\omega(x)$, $\phi(x)$ and ζ are respectively eigenfrequency, modal radial displacement magnitude under tool tip and damping for given eigenmode, dependent from the axial tool position x.

6. Results and discussion

The Figure 7 features stability lobes charts for two different tool positions x. One can notice that as the tool progresses, the lobes shift down and left. Thus, the point representing our system meets different lobes during the pass. In our case the rotation rate is constant during the pass and the stability chart can be presented as a function of x. The assembly of the stability lobe

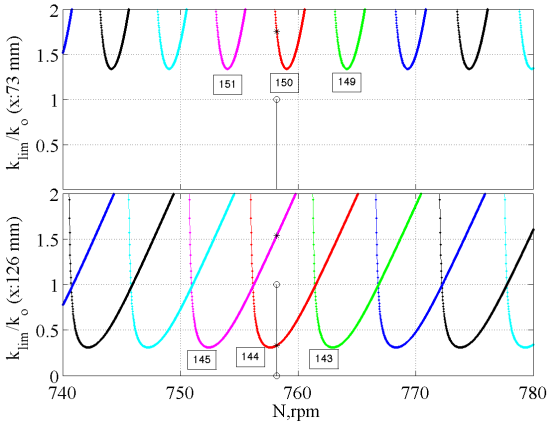

Fig. 7. Stability lobes charts for different tool positions x

slices corresponding to $\Omega = 758.15$ rev/min for various tool positions x is presented on the top chart in Figure 8. This result is in agreement with the experimental data shown below on the same figure: the eigenfrequency $\omega(x)$ remains close to the resonance frequency that can be observed on the spectrogram. Moreover, the intermittent character of the vibrations that can be observed in the time and frequency domain data can be explained by exiting stability lobes. The location and the vibrated areas on the machined surface (see Figure 2) would correspond to the high-magnitude vibration bursts and to resonance spots on the spectrogram.

One can notice that the resonance frequency evolution is not continuous but rather has a "stair-case"-shaped pattern, with each step height close to 12Hz which corresponds to the workpiece rotation frequency.

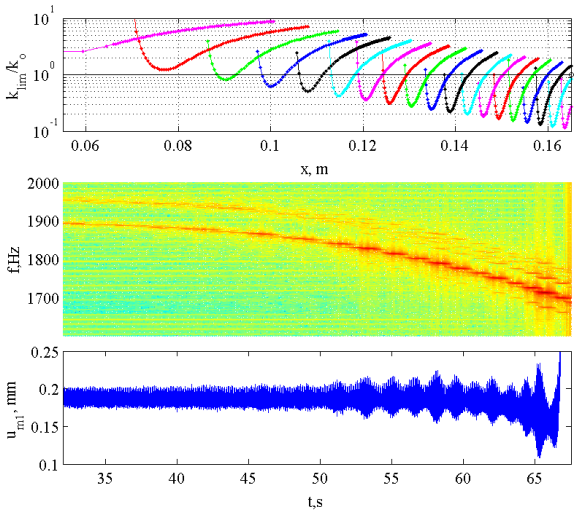

Fig. 8. Evolution during the last tool path of the stability limit (top) for Ω = 758.15 rev/min, the spectrogram (middle) and the displacement at 'm1' (bottom)

Such pattern is in agreement with the fact that the eigenfrequency varies in quite a large range (from 1940 down to 1660 Hz which would correspond to the number of lobes the system goes through during the pass). It is of interest to notice that for $x > 120$ mm the system evolves continuously in the unstable zone. Nevertheless, when leaving one instability zone, the system changes discontinuously the response frequency.

Finally, it can be observed that the uncertainty on the system's constitutive properties can also impact the resulting machined surface in a discontinuous way: on Figure 9 one can see that a 30% variation in damping can quite easily add to or diminish the occurrence of the instability zones.

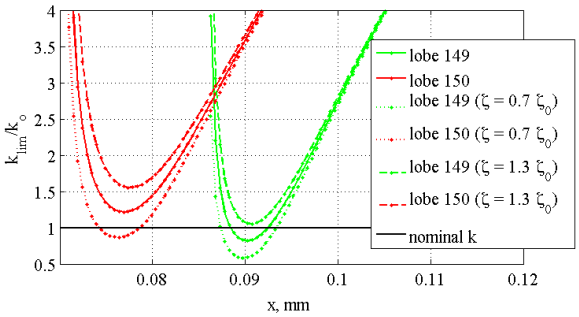

Fig. 9. Stability limit evolution during for different damping values

7. Conclusion

An experimental investigation of a straight turning operation on a thin-walled structure (tube) reveals the instabilities of the quasi-steady cutting under variable conditions, due to the structure's mass and compliance variation. A numerical modeling of the workpiece including variable thickness enables the reproduction of the system's eigenfrequencies which are visible as resonances in the experimental data. A general modal approach for the stability evaluation is developed. In our case, the system's behavior concerning the instability, proves to be relevantly reproduced using only one eigenmode. This framework enables an insight into the intermittance of the stationary cutting. However, the accuracy of system's constitutive parameters is important in order to detect correctly the instability areas.

References

[1] Tobias S. A. and Fishwick W. A theory of regenerative chatter. The Engineer. London; vol. 205:139–239, 1958.
[2] Gmür T. Dynamique des Structures – Analyse modale numérique. Presses Polytechniques et Universitaires Romandes (EPFL); 2008.
[3] Altintas Y. Manufacturing automation. Cambridge University Press; 2000.
[4] Jayaram S, Kapoor SG, and Devor RE. Estimation of the specific cutting pressures for mechanistic cutting force models. Int. J. Mach. Tools & Manufacturing 2001; 41/2 :265–281.
[5] Kienzle O. Die Bestimmung von Kräften und Leistungen an spänenden Werkzeugen und Werkzeugmaschinen. Z-VDI 1951; 94 :299–305.
[6] Altintas Y. Manufacturing Automation: Metal Cutting Mechanics. Machine Tool Vibrations, and CNC Design. Cambridge University Press; 2012.
[7] Cheng K. Machining Dynamics: Fundamentals, Applications and Practices. Springer; 2008.
[8] Siddhpura M, Paurobally R. A review of chatter vibration research in turning. International Journal of Machine Tools and Manufacture; 2012; 61:27–47.
[9] Arnold RN. Chatter Patterns Formed on the Surface of Thin Cylindrical Tubes during Machining. Journal of Mechanical Engineering Science; 1961; 3:7–14.
[10] Mehdi K, Rigal JF, Play D. Dynamic behavior of a thin-walled cylindrical workpiece during the turning process, Part 2: Experimental approach and validation. Journal of manufacturing science and engineering; 2002; 124:569–580.
[11] Mehdi K, Rigal JF, Play D. Dynamic behavior of a thin-walled cylindrical workpiece during the turning process, Part 1: Cutting process simulation. Journal of manufacturing science and engineering; 2002; 124:562–568.
[12] Lorong P, Larue A, Perez Duarte A. Dynamic Study of Thin Wall Part Turning. 13th CIRP International Conference on Modeling of Machining Operations, Advances Materials Research. 2011; Sintra, Portugal.